Discussion on feasibility of inserting the GSP into LCOS

Ni Lei[1,2], Shen Chuan[1], Li Hao[1], Liu Kaifeng[1], Wei Sui[1]

(1. Key Laboratory of Intelligent Computing & Signal Processing, Anhui University, Hefei 230039, China;
2. Key Laboratory of Modern Imaging and Displaying Technology of Anhui Province, Hefei 230039, China)

Abstract: The liquid crystal on silicon (LCOS) is one of the most appropriate spatial light modulators for holographic video display but the off-the-shelf LCOS is not suited because of mainly its small diffraction angle and low resolution. Metasurface, for example, gap-surface plasmon (GSP), has recently emerged as an innovative approach to control light propagation with unprecedented capabilities. In this paper, the feasibility of inserting one kind of metasurface into the LCOS was numerically discussed to deal with the problem. To the practical purpose, aluminum was used as the metal layer, the aluminum oxide layer was used as the insulating layer to form GSP structure. Firstly, the optical properties of aluminum at visible frequencies and the relative Fabry-Perot resonator model were studied. The preliminary structure then was inserted into LCOS to observe its effects on the electric field in the liquid crystal and consequently the changes of the liquid crystal director. The numerical simulations results show that the proposed structure has some influence on the diffraction of the far-field light and there are some changes in the viewing angle of the holographic display. The purpose of inserting the GSP into LCOS devices proposed here is technically feasible.

Key words: holographic video display; liquid crystal on silicon; gap-surface plasmon; Fabry-Perot resonator model

CLC number: TN2 **Document code:** A **Article ID:** 1007-2276(2015)06-1773-05

GSP 插入 LCOS 的可行性探讨

倪 蕾[1,2],沈 川[1],李 浩[1],刘凯峰[1],韦 穗[1]

(1. 安徽大学 计算智能与信号处理教育部重点实验室,安徽 合肥 230039;
2. 安徽省现代成像和显示技术重点实验室,安徽 合肥 230039)

摘 要: 硅基液晶(LCOS)是最适合用于全息视频显示的空间光调制器之一,但是受限于小衍射角和低分辨率的特性,当前市场上的 LCOS 并不完全适用。近年来出现的超常表面(例如,间隙表面等离子体激元) 具有独特的特性, 提供了一种新的对光传播进行控制的方法。文中采用数值方法研究了在 LCOS 中插入超常表面结构,旨在解决小衍射角和低分辨率的问题。为了实用化,使用铝作为金属层、三氧化二铝层作为电介质层,生成 GSP 结构。首先,研究了铝在可见光频率的光学特性以及相应的法布里珀罗共振子模型。然后将初始 GSP 结构插入到 LCOS 中,得到液晶中的电场分布,进一步观察液晶中指向矢分布的变化。数值模拟的结果表明,所提出的结构对远场衍射光具有一定的影响,并且全

收稿日期:2014-10-12; **修订日期**:2014-11-15

基金项目:国家自然科学基金(61377006, 61301296, 61201396);国家自然科学基金-广东联合基金(U1201255)

作者简介:倪蕾(1989-),女,硕士生,主要从事全息显示方面的研究。Email:nl40614078@163.com

导师简介:韦穗(1946-),女,教授,博士生导师,主要从事计算视觉与三维全息显示方面的研究。Email:swei@ahu.edu.cn

息显示的视场角也发生一些改变。因此,这里提出的在 LCOS 装置中插入 GSP 的方案在技术上是可行的。

关键词:全息视频显示; 硅基液晶; 缝隙表面等离子体; 法布里珀罗共振子模型

0 Introduction

The liquid crystal on silicon (LCOS) is the marriage of flat-panel display and COMS technology, so it gets benefit from both sides. It is one of the most appropriate spatial light modulators for holographic video display. However, the off-the-shelf LCOS can only be used as a proof of concept device, because of the characteristics of low-band width and small diffraction angle. The pixel size of SLM needs to close to the scale of visible light wavelength to provide the desired viewing angle in holographic display[1-2]. Unfortunately, as mentioned in[3] that a small pixel spacing in liquid crystal device will make the inter pixel coupling caused by fringing field is a non-negligible issue. This results in modulation depth reduction and higher diffraction loss to unwanted diffractive orders.

Recently metasurface[4-6], plasmonic arrays with periodicity sub-wavelength scale, has emerged as an innovative approach to control light propagation with unprecedented capabilities, it may open a new way to conquer the difficulty in design the LCOS specifically for meeting the need of the viewing angle of the holographic display.

In this paper, a GSP structure is proposed to insert into the LCOS devices for the purpose of investigating the possibility of realizing large diffraction angle and high efficiency. To match the material used in LCOS, the optical properties of aluminum at visible frequencies and the relative Fabry-Perot resonator model are studied instead of noble metal most widely used in lectures. The preliminary structure then is inserted into LCOS to observe its effects on the electric field in the liquid crystal and consequently the changes of it. Here, the liquid crystal (LC) molecular director orientation is determined by TechWiz LCD software and the whole optical properties are calculated by FDTD Solutions software. The numerical simulations show that the proposed structure has some influence on the diffraction of the far-field light. Compared with the conventional LCOS device, it is inferred that there are some changes in the viewing angle of the holographic display. The combination of the GSP and the LCOS devices proposed here is technically feasible.

1 Optical properties of aluminum and aluminum oxide

The fundamental theory of metasurface is related to the optical properties of metal[7]. The optical properties of metal are determined by the conduction electrons that move freely within the bulk of material, while the energy of the photons exceeds the band gap energy of the respective metal occurs inter band excitation. The conduction electrons in a real metal may be excited by an external light field.

Over a wide frequency range, the optical properties of excitation could be explained by a plasma model. The models currently used in the analysis of metal surface plasmon dispersion are Lorentz model, Debye model, Drude model and the Drude-Lorentz model[8-11]. Taking the contribution of free electrons and the harmonic oscillator into account, the Drude-Lorentz model is an efficient and accurate model to describe the dielectric functions of metal. The Drude model, also known as the free electron gas model, whose metal electrons are seen as an ideal gas consisting of electrons is a classic free-electron model that can be used in free-electron metals. The Drude-Lorentz model and the Drude model are given as Eq.(1) and Eq.(2), respectively.

$$\varepsilon_{D-L}(\omega)=\varepsilon_{\infty}-\frac{\omega_p^2}{\omega^2+i\omega\gamma_{fe}}+\sum_{j=1}^{J}\frac{\omega_{Pj}^2}{\omega_j-\omega^2-i\omega\gamma_j} \quad (1)$$

$$\varepsilon_D(\omega)=\varepsilon_{\infty}-\frac{\omega_p^2}{\omega^2+i\omega\gamma_{fe}} \quad (2)$$

where ε_{∞} is the relative permittivity at infinite frequency; ω_p is the plasma frequency represents the natural frequency of the oscillations of free electrons and γ_{fe} denotes the damping constant of the free electron; ω is the angular frequency of the optical wave; ω_{Pj}, ω_j and γ_j denote the plasma frequency, resonance frequency and damping constant of the oscillator, respectively.

It is important to select the suitable plasma material for specific applications. As we know, gold and copper have very similar dielectric constants at the wavelength more than 600 nm[11]. Silver at wavelengths of 450−550 nm is better than gold. The aluminum has a larger (negative) real part of the dielectric permittivity. Therefore, it is one of the most desirable metal, particularly in the 400−600 nm spectral domains. Its attractive properties include low cost, high natural abundance, and ease of processing by a wide variety of methods. At very short wavelengths below 400 nm, the Lorentz resonances are noticeable. But what we care about are the cases in visible wavelengths, so Drude model is used for our research. The curves of permittivities of the aluminum, gold and silver in the Drude model and the Drude-Lorentz model at the optical wavelengths of 400−700 nm are shown in Fig.1.

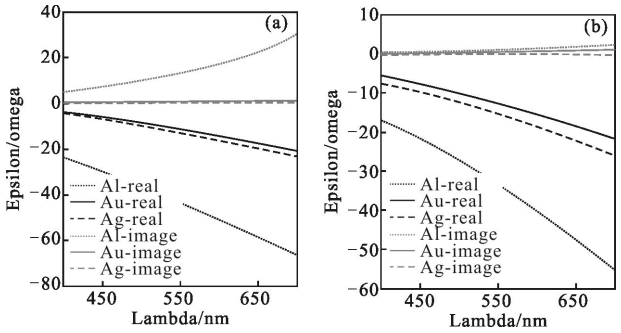

(a) Dielectric permittivities calculated by the Drude-Lorentz model

(b) Dielectric permittivities calculated by the Drude model

Fig.1 Curves of dielectric permittivities of the aluminum, gold and silver at optical wavelengths of 400−700 nm

2 Structure of metal-insulator-metal(MIM)

Plasma model or surface plasmon polaritons (SPP) are optically excited, which are coupled to surface collective oscillations of free electrons in a metal, propagated along metal-dielectric interfaces. Here, the basic properties of the propagating SPP on the metal-dielectric interfaces are described and aluminum is used instead of noble metal usually found in lectures[12−16].

2.1 Aluminum-aluminum oxide

Firstly, we calculate the SPP propagating and decaying in a single aluminum-aluminum oxide interface. The SPP described here at a metal-dielectric interface z=0, are Transverse Magnetic (TM) waves which are exponentially decay with the distance from the interface in both region. We assume the TM wave is propagating along the x-axis. So, the electric field has x-and z-components, and the magnetic field only has a y−component.

We substitute the index m and d for the metal and dielectric in this paper, respectively. From the equality of continuous tangential components of the electric field and the equality of the tangential component of magnetic field at the interface, we have the surface waves propagating along the interface.

$$K_S \equiv k_{x,m}=k_{x,d}=k_S+i/2L_S \quad (3)$$

$$\frac{k_{z,m}}{\varepsilon_m}=-\frac{k_{z,d}}{\varepsilon_d} \quad (4)$$

It is necessary that the real part of dielectric constants for the two media have opposite signs for the wave decays exponentially in both regions. We find the SPP k −vector using the momentum conservation in both media,

$$\varepsilon_m k_0^2=K_S^2-k_{z,m}^2 \quad (5)$$

$$\varepsilon_d k_0^2=K_S^2-k_{z,d}^2 \quad (6)$$

where $k_0=\omega/c$, so the dispersion relation of SPP is

$$K_S(\omega)=k_0(\omega)\sqrt{\frac{\varepsilon_m(\omega)\varepsilon_d(\omega)}{\varepsilon_m(\omega)+\varepsilon_d(\omega)}} \quad (7)$$

2.2 Aluminum-aluminum oxide-aluminum

Considering the geometry that a thin dielectric

layer be sandwiched between two metal surfaces, we find that the SPP modes can be supported by MIM structures. Assuming SPP wave with $k-$vector $K_S=k_{x,i}$ ($i=m,d$) is propagating along the $x-$axis. From the continuity of the tangential components of the magnetic field and electric field and according to the momentum conservation, $k_{z,i}^2=K_S^2-\varepsilon_i k_0^2$, the dispersion relation for dual interface SPP could be written as

$$\left(\frac{k_{z,m}}{\varepsilon_m}+\frac{k_{z,d}}{\varepsilon_d}\right)=\pm\left(\frac{k_{z,m}}{\varepsilon_m}+\frac{k_{z,d}}{\varepsilon_d}\right)\exp(-k_{z,d}t) \tag{8}$$

For Eq.(8), while the thickness of the dielectric t tending to infinity, the right part of the equation becomes zero and we can notice for each interface there is one SPP mode. So, the two SPP modes start to couple and hybridize into a new SPP mode (MIM SPP) when the thickness decreases.

2.3 Fabry-Perot resonator model

TM wave propagating along the $x-$axis and the metal structures are finite width along the $x-$axis[17-20]. The SPP wave propagates forward and backward along the $x-$axis forming standing wave resonance for certain wavelength. The resonance position of the standing-wave can be described by Fabry-Perot resonator formula:

$$w\frac{2\pi}{\lambda}n_{\text{spp}}=m\pi-\phi \tag{9}$$

where w is the width of the resonator, n_{spp} is the real part of effective refractive index of the SPP, is an integer, ϕ is the an additional phase shift related to reflection of SPP at the resonator terminations.

For the effective refractive index of the SPP is acquired upon the $k-$vector of a SPP wave K_S. From the Eq.(8) and the momentum conservation, $k_{z,i}^2=K_S^2-\varepsilon_i k_0^2$, at unique light wavelength and the fixed width of the aluminum, the change of the thickness of the dielectric may affect the SPP resonator.

3 Numerical simulations and results

In the view of MIM structures as GSP resonators, we numerically simulate the possibility of inserting the GSP into the LCOS devices. In this paper, TechWiz LCD software is used to determine the liquid crystal director orientation and the electric field lines in the LC layer for a LCOS cell with the pixel size 3.74 μm, and then the optical performance of the model is calculated with FDTD Solutions software.

The LC material used for determining the molecular orientation here is E7 (Merck). The twist angle and pre-tilt angle are assumed to be 0° and 2°, respectively. Cell thickness is set as 2.5 μm. The voltage between the adjacent pixels are equal in our experiments. For all the optical simulation, the wavelength of incident plane wave is 632.8 nm, incident light is TM polarized and propagates along the $x-$axis.

The schematic diagrams of the typical geometry of LCOS cell we used are shown in Fig.2. Fig.2(a) shows the cell structure of typical geometry LCOS, and the LC director profile shown in Fig.2(b). Due to the limitations convergence ability of TechWiz LCD software, let 1.4 μm be the pixel size of the LCOS cell. Similarly, Fig.3 shows the sketch of the preliminary cell structure which is constructed by inserting the structure into each pixel of the LCOS. Fig.3(a) is the sketch of the preliminary cell structure, and Fig.3(b) is the LC director orientation profile under a static voltage of V=3 V.

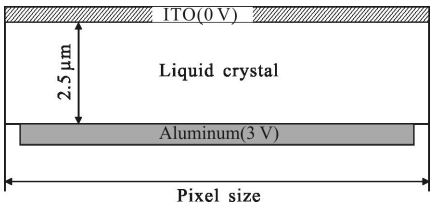

(a) Cell structure

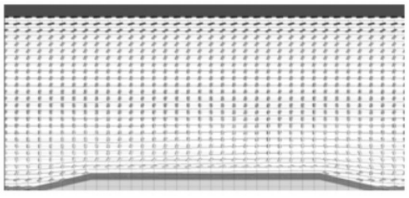

(b) Distribution of LC director orientation

Fig.2 Typical geometry of LCOS

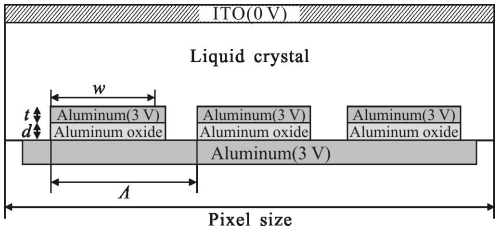

(a) Sketch of the preliminary cell structure

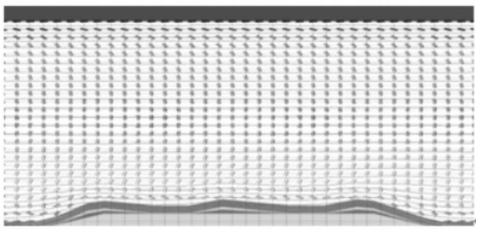

(b) Distribution of LC director orientation

Fig.3 Preliminary structure that insert a structure into LCOS

Comparing the discrete distribution of LC director orientation of Fig.2(b) with Fig.3(b), it is clearly that the difference is very small, at the order of 0.01. For simplicity, assume that the inserted structure does not affect the discrete distributions of the electric field and LC director orientation for larger size of pixel cell (3.74 μm).

After the properties of LC director is discussed, now we turn our attention to optical performance of our structure. First, while the pixel size of the cell is 3.74 μm, the width of the aluminum electrode is 3.54 μm, the thickness of the LC layer is 2.5 μm, and the applied voltage is 3 V. Fig.4(a) is the sketch of the cell of the original LCOS and Fig.4(b) illustrates the normalized diffraction efficiency of different angle, the angle of the diffraction order is about 9.5°.

Now, concerning the basic unit cell of our model, as shown in Fig.5, we fix the period equal to 177 nm, the aluminum oxide thickness d=40 nm, the upper aluminum height t=30 nm and the lengths of five upper aluminum cell are set as 97, 85, 74, 58 and 14 nm, respectively. Such a design can ensure that the reflection phase for TM polarization is dispersed into six pieces by 30° each step. The super cell period of 885 nm (5×177 nm=885 nm) that causing normal incident light to be reflected into first diffraction order at the angle of 45°, meaning there are four basic unit cell of our model on the aluminum electrode of the width 3.45 μm. The incident field is TM polarized and propagates normal to the surface. The performance of the designed structure is studied numerically. It is obviously that in Fig.4 (b). The angle of light scattered by the metasurface is about 42° which is closely agreement with the ±1 diffraction order angle (for period of 885 nm).

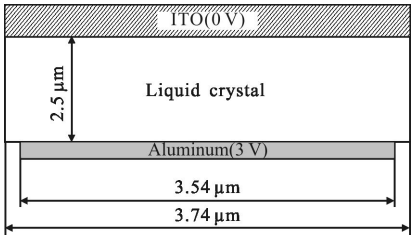

(a) Sketch of the cell

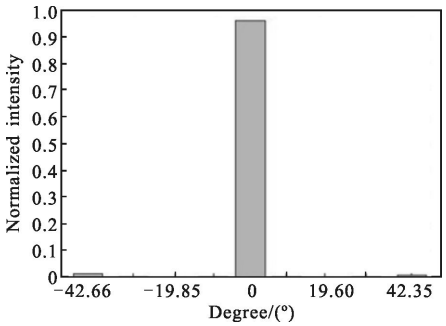

(b) Normalized diffraction efficiency of different angles

Fig.4 Original geometry of LCOS

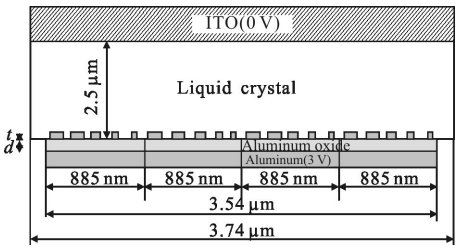

(a) Sketch of the unit cell

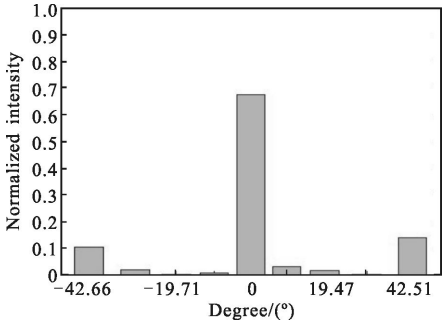

(b) Normalized diffraction efficiency of different angles

Fig.5 Proposed structure of our model

4 Conclusion

The distributions of the LC director orientation are simulated and the optical properties of the proposed structure are calculated in this paper. The proposed structure has little influence on both the distributions of the electric field and LC director orientation but increases the angle of the diffraction light compared with original LCOS device. In future, we would like to use Comsol Software to do more accurate simulation in the discrete distributions of the electric field and optimize the width of the metal and the thickness of the dielectric at various wavelengths.

References:

[1] Smalley D E, Smithwick Q Y J, Bove V M, et al. Anisotropic leaky-mode modulator for holographic video displays[J]. ***Nature***, 2013, 498(7454): 313-317.

[2] Stahl R, Rochus V, Rottenberg X, et al. Modular sub-wavelength diffractive light modulator for high-definition holographic displays [C]//Journal of Physics: Conference Series. IOP Publishing, 2013, 415(1): 012057.

[3] Michalkiewicz A, Kujawinska M, Kozacki T, et al. Holographic three-dimensional displays with liquid crystal on silicon spatial light modulator [C]//Optical Science and Technology, the SPIE 49th Annual Meeting. International Society for Optics and Photonics, 2004: 85-94.

[4] Pors A, Bozhevolnyi S I. Plasmonic metasurfaces for efficient phase control in reflection[J]. ***Optics Express***, 2013, 21(22): 27438-27451.

[5] Lal S, Link S, Halas N J. Nano-optics from sensing to waveguiding[J]. ***Nature Photonics***, 2007, 1(11): 641-648.

[6] Knight M W, Liu L, Wang Y, et al. Aluminum plasmonic nanoantennas[J]. ***Nano Letters***, 2012, 12(11): 6000-6004.

[7] Caldwell M E, Yeatman E M. Surface-plasmon spatial light modulators based on liquid crystal [J]. ***Applied Optics***, 1992, 31(20): 3880-3891.

[8] Schulz L G, Tangherlini F R. Optical constants of silver, gold, copper, and aluminum. II. The index of refraction n [J]. ***JOSA***, 1954, 44(5): 362-367.

[9] Chan G H, Zhao J, Schatz G C, et al. Localized surface plasmon resonance spectroscopy of triangular aluminum nanoparticles [J]. ***The Journal of Physical Chemistry C***, 2008, 112(36): 13958-13963.

[10] Farhad Shokraneh. Scattering Properties of Nanoantennas[M]. Sweden: Department of Electrical and Information Technology Lund University, 2012.

[11] Biagioni P, Huang J S, Hecht B. Nanoantennas for visible and infrared radiation [J]. ***Reports on Progress in Physics***, 2012, 75(2): 024402.

[12] Bozhevolnyi S I. Plasmonic Nanoguides and Circuits [M]. Denmark: Optical Society of America, 2008.

[13] Chan G H, Zhao J, Schatz G C, et al. Localized surface plasmon resonance spectroscopy of triangular aluminum nanoparticles [J]. ***The Journal of Physical Chemistry C***, 2008, 112(36): 13958-13963.

[14] Gjonaj B. Digital plasmonics: from concept to microscopy [D]. Netherlands: FOM Institute for Atomic and Molecular Physics Science Park, 2012.

[15] Encina E R, Coronado E A. Plasmonic nanoantennas: angular scattering properties of multipole resonances in noble metal nanorods [J]. ***The Journal of Physical Chemistry C***, 2008, 112(26): 9586-9594.

[16] Zhu Jun , Li Zhiquan, Qin Liuli. Cavity physical properties of SPP propagation in the MIM structure [J]. ***Infrared and Laser Engineering***, 2015, 44(3):852-856. (in Chinese)

[17] Barnard E S. Plasmonic optical antennas for enhanced light detection and emission [D]. America: Stanford University, 2011.

[18] Sϕndergaard T, Bozhevolnyi S I. Strip and gap plasmon polariton optical resonators [J]. ***Physica Status Solidi (b)***, 2008, 245(1): 9-19.

[19] Yang J, Sauvan C, Jouanin A, et al. Ultrasmall metal-insulator-metal nanoresonators: impact of slow-wave effects on the quality factor [J]. ***Optics Express***, 2012, 20 (15): 16880-16891.

[20] Liaw J W, Huang C H, Chen B R, et al. Subwavelength Fabry-Perot resonator: a pair of quantum dots incorporated with gold nanorod [J]. ***Nanoscale Research Letters***, 2012, 7(1): 1-7.